Available online at www.sciencedirect.com
ScienceDirect
Journal of the European Ceramic Society 27 (2007) 1615–1622
www.elsevier.com/locate/jeurceramsoc

Thermal spraying to coat traditional ceramic substrates: Case studies

C. Bartuli [b], L. Lusvarghi [a,*], T. Manfredini [a], T. Valente [b]

[a] *Dipartimento di Ingegneria dei Materiali e dell'Ambiente, Università di Modena and Reggio Emilia, Via Vignolese, 905-41100 Modena, Italy*
[b] *Dipartimento di Ingegneria Chimica e dei Materiali, Università degli Studi di Roma "La Sapienza", Via Eudossiana, 18-00184 Roma, Italy.*

Available online 9 June 2006

Abstract

Thermal spray is a group of continuous, line of sight, deposition methods, where usually particles (1–50 μm) are melted and accelerated, through either a combustion or a plasma flame. The molten droplets impinge on a substrate and rapidly solidify to form thin layers ("splats"). Among these techniques, plasma spraying is particularly fit for spraying ceramics and applied in many industrial applications on metallic surfaces. However, it has seldom been used for spraying glasses and even less to coat ceramic substrates, in particular traditional ones. In this paper, layered refractory ceramics coatings on sintered refractories have been deposited to improve the substrate resistance to molten glass. Some examples of plasma sprayed high-performance or waste glasses applied on porcelanized stoneware and porous single-firing bodies are presented, too. The coatings have been subsequently thermally treated and microstructural, chemical, mechanical analysis have been carried out both on as-sprayed and treated samples.

Keywords: Plasma spraying coatings; Glass ceramics; Refractories; Glass; Traditional ceramics

1. Introduction

Thermal spraying coating processes use a flux of gases, heated by a thermal source (usually a combustion within the gas or a DC or RF electric arc), to melt and accelerate droplets of the coating material towards the substrate. The plasma spraying technique generates a hot plasma in a flux of high-pressure (>1 bar) gases by striking an electric arc between a tungsten cathode and a copper anode/nozzle in a plasma torch.[1] The coating material, generally in powder, is injected in the plasma jet; significant feeding parameters include injector position and diameter and carrier gas flow rate.[2]

Melted particles flatten and solidify upon impact with the substrate, assuming a lamellar morphology (splats); their rapid cooling causes high tensile stresses leading to microcracking in brittle materials.[3] Due to the microcracks, to the relatively low particles speed, to unmolten particles and gas entrapment, plasma sprayed coatings generally possess a porosity >4%.[4] The very high plasma temperature enable the deposition of high-melting-point ceramics, with several applications which concerns automotive, aerospace, electronic, printing industry, corrosion control, metal processing, textile and polymer industries,[5] usually dealing only with metallic substrates. This work shall study three particular cases of functional ceramic coatings on ceramic substrates. The first study concerns coated refractories, which have to resist chemical attack and wear phenomena occurring in processing plants by molten materials (glass manufacturing plants, primary metallurgy plants). This research suggests that coated sintered refractories could partly replace expensive electro-fused ones used in glass processing furnaces. The other two cases illustrate the promising employment of plasma spraying as an alternative to traditional ceramic glazing technique. The coating material melting temperature can be higher than the substrate and their thermal expansion coefficients can be significantly different, because the coating material is molten during spraying while the substrate remains at low temperature.[6]

2. Common materials and methods

In this paragraph the standard procedures are reported; the others analysis performed for the single case studies will be described in the relative sections. The coatings have been plasma sprayed in air plasma spraying (APS) mode, with a C.A.P.S. plant equipped with a Sulzer Metco F4-MB plasma torch with a 6 mm diameter nozzle (C.S.M. S.p.A., Roma, Italy, co-shared with Università "La Sapienza", Rome, Italy). The substrates have previously been grit-blasted with a vacuum operated

* Corresponding author. Tel.: +39 05 92056206; fax: +39 05 92056243.
E-mail address: lucalusv@unimore.it (L. Lusvarghi).

0955-2219/$ – see front matter © 2006 Elsevier Ltd. All rights reserved.
doi:10.1016/j.jeurceramsoc.2006.05.049

Norblast blasting machine, with alumina grits (Sulzer Metco Metcolite-C). Cross-sectional coatings samples were cut from the coated materials, cold-mounted in resin, ground with 400, 800, 1000 mesh SiC papers, polished with 3 and 0.5 μm diamond paste and observed through scanning electron microscopy (SEM XL30, Philips). Image analysis was performed on 400× and 1000× SEM micrographs (UTHSCSA Image Tool 3.0) to assess the porosity; X-ray diffraction (PW 3710, Philips, Cu Kα radiation) was performed on the upper and lower surfaces of the coatings to determine the crystalline phases. The HX1000 microindenter (Remet) was employed to measure Vickers microhardness on polished cross-sections; high-load cracked Vickers microindentations on the cross-sections were employed in fracture toughness measurement (according to literature studies[7,8]) through the Evans-Charles and Evans-Wilshaw formulae. All indentations and cracks were measured from SEM images; at least 15 indentations have been performed in both cases. Dry particles abrasion resistance of coated samples was tested by means of a dry particles – steel wheel test (Ceramic Instruments AP/87), with a Fe360 steel wheel rotated at 75 rpm and pressed by a 40.2 N normal load against the sample surface in presence of a tangential flux (1 g/disk revolution) of corundum particles (FEPA 80: 180 μm mean particle diameter). The results are expressed as wear volume/unit sliding distance of the disk (mm^3/m), labelled in the text Vn.

3. Case study no. 1: plasma sprayed coatings on porous refractories for glass furnaces applications

Thermally sprayed coatings have seldom been tested in the contact with chemically aggressive molten materials at high temperature.[9,10] The simultaneous presence of mechanical actions due to convective flows or stirring devices, which occur in molten glass processing plants require the components to have also a good resistance to wear in those demanding conditions. In particular, molten glass processing furnaces generally require the employment of very expensive cast alumina-zirconia-silica refractories, in order to stand the chemical action of molten glass.[11] Sintered ceramics (which would cost up to 15–20 times less) are also employed in such applications, even though they are much more vulnerable than electro-fused ones, because the glass can easily start percolating through the interconnected porosity and dissolving the material. If a low porosity, chemically resistant, thick pure alumina coating could be deposited onto the surface of a sintered refractory brick, it could significantly hinder molten glass percolation and consequently delay the refractory dissolution. In this study, some low cost alumina-mullite sintered refractories were coated by means of plasma spraying, aiming at the production of a pure alumina top coating. To lessen the thermal expansion coefficient mismatch between alumina and the porous substrate, graded coatings have been designed: underlying alumina-mullite layers have been sprayed before the alumina top coat, exploiting the low thermal expansion coefficient of mullite.

A commercial alumina-mullite based sintered refractories, with commercial designation EXTRA55, supplied as (220 mm × 110 mm × 60 mm) bricks, has been employed in this study. Its nominal chemical composition is 55% Al_2O_3, 40% SiO_2 and zircon and ematite up to 100%. It is coefficient of thermal expansion is $5.73 \times 10^{-6}\,C^{-1}$ ($200\,^{\circ}C < T < 1200\,^{\circ}C$) and a porosity value around 20%. Three commercially available thermal spray ceramic powders have been employed for coatings production: a $-45 + 15$ μm mullite powder (Saint Gobain #1020), a $-45 + 15$ μm alumina powder (Saint Gobain #153PT) and a $-31 + 3.5$ μm alumina powder (Sulzer Metco 105SFP). The plasma spraying deposition parameters are: 6 mm torch nozzle; 100 mm spray distance; 500 mm/s torch traverse speed; Ar (50 Slpm)/H_2 (15 Slpm) plasma gas mixture; 40.95 kW overall power input for the composite layers and 39 kW for the alumina top coating.

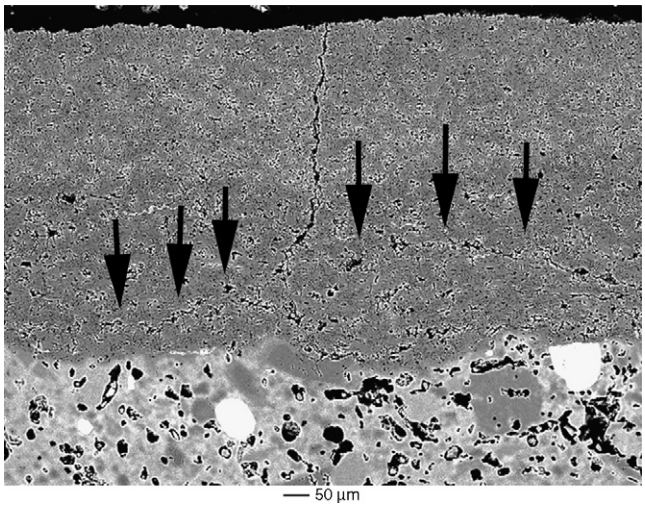

Fig. 1. Three-layered coating after the 3rd cycle during the thermal shock tests; the black arrows indicate the deflected cracks parallel to the substrate.

To effectively evaluate the thermal expansion coefficients (CTE) of alumina and mullite, a recently patented and manufactured non-contact optical dilatometer (Misura ODLT, Expert System Solutions, Italy) has been employed (Fig. 1). The thermomechanical behaviour of (50 mm × 10 mm × 1 mm) self standing plasma sprayed samples (deposited with the same coating's parameter), placed into a furnace, is investigated by means of two beams of light illuminating both the ends of it and two digital cameras capturing the images of the last few hundred microns of each tip. All the coatings were subjected to cyclic thermal shock testing: five (60 mm × 20 mm × 10 mm) samples were cut from the coated plates, heated in an electric kiln at 15 °C/min up to 1400 °C, left at 1400 °C for 30 min, rapidly extracted and left in air at room temperature for 30 min in order to cool them down completely. Sample number 1 was then removed and analysed, while the others were subjected to further thermal shocks by inserting them into the kiln (which has been left at the chosen operating temperature) for 30 min and pulling them out again, that is at room temperature. The chemical resistance of coatings to molten glass was also tested. A frit employed in metals glazing, chemically very aggressive due to the presence of significant amounts of Na_2O, CaO, NiO, MnO_2, Fe_2O_3, ZnO, CoO, was used. Powders obtained by ball milling the frit were laid onto a coated sample; the sample was then put into

an electric kiln, heated up to 1400 °C at 15 °C/min, left at the operating temperature for 8 h, then slowly cooled down inside the kiln. Uncoated refractory samples were also tested for reference. The thermal shock and the chemical resistance tests have been also combined to evaluate the effectiveness of the coatings once damaged by abrupt temperature jumps.

The CTE is a very important parameter, because it constitutes the basis for the layered coatings design. In order to design the layer sequence, a modified rule of mixtures approach[12] was adopted to qualitatively estimate the thermal expansion coefficients of alumina-mullite composite layers, i.e.

$$\alpha_c = \frac{E_{\text{alumina}}\alpha_{\text{alumina}}V_{\text{alumina}} + E_{\text{mullite}}\alpha_{\text{mullite}}V_{\text{mullite}}}{E_{\text{alumina}}V_{\text{alumina}} + E_{\text{mullite}}V_{\text{mullite}}} \quad (1.1)$$

where α_c is the thermal expansion coefficient of the composite layer [°C^{-1}]; E_{alumina}, E_{mullite}, Young's moduli [GPa], α_{alumina}, α_{mullite}, thermal expansion [°C^{-1}], and V_{alumina}, V_{mullite}, are the volume fraction of the constituents.

Two systems have been designed, as above mentioned. One is a two-layered coating: a 70 vol.% alumina–30 vol.% mullite 300 μm-thick layer and an alumina 700 μm-thick upper layer. Assuming $E_{\text{mullite}} = 25$ GPa and $\alpha_{\text{mullite}} = 4.8 \times 10^{-6}$ °C^{-1} for fully crystallized plasma sprayed mullite[13] and $E_{\text{alumina}} = 63$ GPa and $\alpha_{\text{alumina}} = 7.24 \times 10^{-6}$ °C^{-1} for as-sprayed alumina,[14] the thermal expansion coefficient of the composite layer is $\alpha = 6.9 \times 10^{-6}$ °C^{-1} from Eq. (1.1); thus, the mismatch between the lower and upper layer is reduced down to 0.35×10^{-6} °C^{-1}, but the mismatch with the substrate is still high. The second one is a more complex multi-layered system designed so that the mismatch between adjacent layers never exceeds 0.7×10^{-6} °C^{-1}; thus, a three-layers coating has been designed for the EXTRA55 substrate with a 350 μm-thick alumina top layer, a 100 μm-thick 70 vol.% alumina–30 vol.% mullite layer ($\alpha_c = 6.9 \times 10^{-6}$ °C^{-1}), and a 150 μm-thick 35 vol.% alumina–65 vol.% mullite layer ($\alpha_c = 6.2 \times 10^{-6}$ °C^{-1}). During the spraying process, the feeding disk revolution (rounds/min), compensated for the different deposition efficiency of the three powders, has been 12 for the alumina top layer, 8.4–3 for the 70% alumina–30% mullite layer and 4.2–6.5 for the lower one.

Fig. 1 shows the microstructure of the as-sprayed two-layered coatings; it can be noticed that the alumina top layer has a low porosity microstructure (8%). The lower layer has a slightly more defective microstructure, with higher porosity (16%), which may be due to the larger particle size of the employed powders, non-optimal spraying parameters (in particular, for the two-layered coating, an excessively high 50 kW operating power in the plasma torch was employed), and the different in-flight and solidification progress of mullite and alumina.

The adhesion to the substrate appears to be very good: it can be explained with the extreme roughness/waviness of the grit-blasted bricks and the chemical affinity of the lower layer with the substrate. SEM micrographs analysis has shown no major microstructural differences between the three-layered coatings with the simpler ones. As-sprayed alumina is mainly constituted by its gamma phase, while mullite XRD patterns show a clear broad band indicating the presence of a glassy phase. Since the coated system was going to be thermally treated at high temperature, the optical measurements of CTE has been performed both on as-sprayed and 8 h 1400 °C fired alumina and mullite specimens (Table 1).

Table 1
Measured CTE of free standing plasma sprayed specimen

Free standing specimen	α [$\times 10^{-6}$ °C^{-1}] (25 °C < T < 1000 °C)
As-sprayed alumina	6.94
1400 °C, 8 h alumina	7.69
As-sprayed mullite	4.40*
1400 °C, 8 h mullite	4.93

* This value has been taken in a different temperature range (25 °C < T < 400 °C), to avoid the vitreous phase sintering process and the subsequent crystallization.

The difference between the measured CTE and the ones used to design the coating is considerable only in the alumina case, because the $\gamma \rightarrow \alpha$ phase transition do change the thermomechanical behaviour of the alumina splats, even though the CTE mismatch between adjacent layers is still below 0.85×10^{-6} °C^{-1}. Some sintering process could also occur, leading to the loss of the splat-like microstructure.

After thermal shock tests, in the two-layered coating, no major cracks are present after one cycle, but further cycles cause thermal shock damage. After the second cycle, some cracks are formed; more cracks are present when the samples undergo three cycles; but no more cracks appear in the subsequent cycles. The cracks propagate perpendicularly to the substrate and transversally to the sample longer side; this clearly means that tensile stresses developed in the alumina layer during cooling caused them. Furthermore, cracks in the refractory substrate parallel to the interface exist at the sample ends; they have probably been caused by the high interfacial shear stresses which are developed in these areas. The fact that no coating delamination across the interface took place confirms the strength of the adhesion to the substrate. The three-layered coatings appear to possess an improved thermal shock resistance; in fact, almost no cracks appear even after two cycles, few are present after three cycles, and no more are formed in the following cycles. Furthermore, cracks in the refractory parallel to the interface are absent or definitely smaller. This clearly indicates that the more gradual transition between the thermal expansion coefficient of the substrate and the alumina top coating lessens all the thermal stresses. SEM micrographs of thermal shock microcracks (Fig. 1) highlight a very interesting phenomenon: cracks do not propagate straightforwardly across the coating, as it happened in the former case, but are often deflected upon reaching the lower layers, where they propagate parallel to the substrate (see black arrows). They seem to propagate across the 65 vol.% mullite layer or across the interface with the 30 vol.% mullite layer. A deeper analysis indicates that they mainly cross alumina splats, confirming the former observations concerning the higher alumina tendency to thermal shock cracking. Thus, the three-layered design has allowed to reduce the thermal shock damage, producing in many cases cracks which do not reach the substrate, avoiding the preference of preferential path for the glass to percolate.

The chemically tested uncoated refractories underwent a deep glass penetration, with depths of more than half millimetre to 2 mm. The glass infiltrated the numerous open pores and dissolved the phases with lower chemical resistance, like mullite; consequently, the alumina grains float unsupported in the glass, undergo increasing chemical attack, and are dragged away by convection motions inside the glass itself. The coatings have been very little affected by the molten glass, and fundamentally retained their original structure. Detailed SEM micrographs indicate that significant alterations were caused by glass penetration just down to a depth of about 50 μm. In such very thin layer, alumina reacted with the glass: it was probably partially dissolved and then re-crystallized due to glass saturation, so that large polygonal alumina grains appear. The transition metals present in the glass reacts with alumina forming spinel crystals. In absence of cracks due to thermal damage, which are present in the two-layered coatings, but much more seldom in the three-layered one, the glass attacks the lower layers very mildly; in fact, only in the 30 vol.% mullite layer displays some limited evidence of molten glass alteration, while mullite seems absolutely unaltered in the 65 vol.% mullite layer. The thermomechanical and chemical combined tests highlight what has been just mentioned: if perpendicular cracks caused by thermal shock are present, the glass can find an easier way to reach the susbstrate; if, on the other hand, the cracks are deflected along the mixed layers before reaching the substrate, dangerous damage can be inflicted to mullite splats.

4. Case study no. 2: recycling of CRT-glass by means of plasma spraying

The production of waste glass-alumina composite coating is an example of a glass phase containing coating manufactured by plasma spraying. Each year, in Italy, 210.000 tonnes of glass coming from the dismantling of electronic equipment is collected; 80% of this wastes consists in TV and PC monitors and 85 wt.% of monitors is made of glass.[15,16] Using waste glass as raw material means saving money and contributing to materials recycling. High percentage of waste glasses from cathodic ray tube (CRT glass) of PC and TV together with alumina powder as reinforcement have been mixed in different percentage to produce coatings for tiles industry application with good mechanical properties. Two different reinforcements have been used: a fine, industrially manufactured alumina powder, usually employed in frits production and a commercially available alumina powder for thermal spraying, whose cost is considerably higher than the former one. Along with the experimental characterization, a finite elements modelling has been proposed.

The waste glass has been ball milled and an acceptable size distribution has been obtained by sieving: $-45+15$ μm. The Sulzer Metco 105SFP alumina powder ($-31+3.5$ μm) and a very fine (<10 μm), platelet-shaped, low cost alumina powder (previously spray-dried by a NERO Atomizer, Denmark) were adopted as reinforcement. Since morphology and size of the cheap alumina were detrimental to its flowability, spray-drying has been performed. Porcelanized stoneware substrates were used. The coatings list and the feeding parameters are reported in Table 2. Once measured the thickness of pure glass and pure alumina coatings achieved with the composite coatings spray parameters, feed rates were chosen by adjusting them by the ratio between such thicknesses to take into account the different deposition efficiency of the powders. The plasma spraying deposition parameters are: 6 mm torch nozzle; 100 mm spray distance; 500 mm/s torch traverse speed; Ar (50 Slpm)/H_2 (15 Slpm) plasma gas mixture; 550 A current and 70 V voltage for a 38.5 kW overall power input. The carrier gas has been argon and its flow 3.5 for the glass with Sulzer alumina and for the two alumina powders and 4.0 for the glass with the cheap alumina. Heat treatment tests were also performed in an electric kiln: 15 °C/min heating rate up to 1000 °C, 15 min isotherm, slow cooling inside the kiln. The coating microstructures were studied by SEM and XRD analysis. Cast bulk glass samples have been produced to determine the thermomechanical properties of the waste glass employed in this study, such as thermal expansion coefficient, Vickers microhardness and fracture toughness, elastic modulus and Poisson's ratio. A finite elements modelling has been performed with the aim of investigating the mechanical properties of these coatings. The OOF program[17] is able to map digitised images onto FEM grids; thus relying on real SEM microstructural micrographs. Various authors have already successfully employed OOF to investigate thermal residual stresses,[18] crack propagation mechanisms of heterogeneous systems,[19] thermal barrier coatings.[20] In this study, the elastic modulus, the resid-

Table 2
Nominal % and feeding parameters of the composite coatings

Sample identification	Alumina nominal %	Glass feeding parameters	Al_2O_3 feeding parameters
F	0	Feeding disk speed: 15 rpm	–
SF20	Sulzer, 20	Feeding disk speed: 4.6 rpm	Feeding disk speed: 12.0 rpm
SF40	Sulzer, 40	Feeding disk speed: 8.1 rpm	Feeding disk speed: 8.0 rpm
SF60	Sulzer, 60	Feeding disk speed: 11.4 rpm	Feeding disk speed: 5.0 rpm
SF80	Sulzer, 80	Feeding disk speed: 15.2 rpm	Feeding disk speed: 2.5 rpm
SA	Sulzer, 100	–	Feeding disk speed: 15 rpm
EF20	Spray-dried, 20	Feeding disk speed: 12.0 rpm	Feeding disk speed: 3.0 rpm
EF40	Spray-dried, 40	Feeding disk speed: 6.0 rpm	Feeding disk speed: 9.0 rpm
EF60	Spray-dried, 60	Feeding disk speed: 9.0 rpm	Feeding disk speed: 6.0 rpm
EF80	Spray-dried, 80	Feeding disk speed: 12.0 rpm	Feeding disk speed: 3.0 rpm
EA	Spray-dried, 100	–	Feeding disk speed: 15 rpm

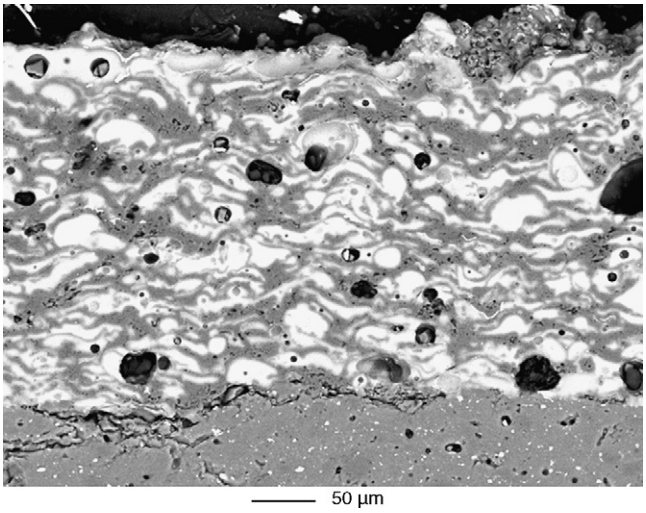

Fig. 2. SEM image of a thermally treated EF 40 coating.

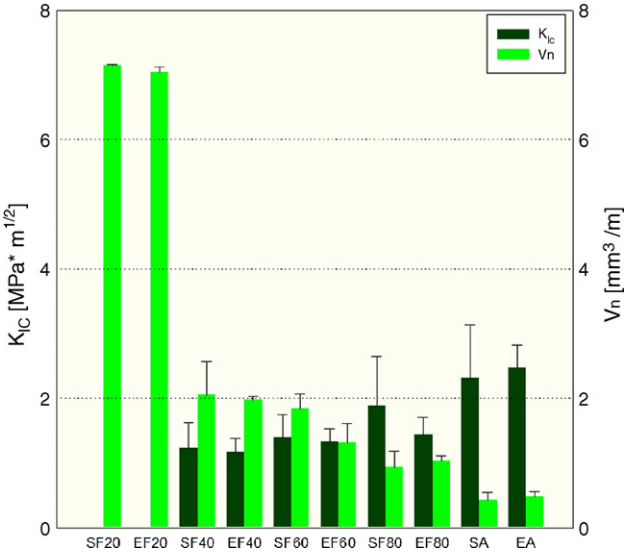

Fig. 3. Mechanical properties of as-sprayed coatings. K_{Ic} is fracture toughness, and Vn is the abrasion rate value.

ual stresses after thermal treatment and the crack propagation behaviour were determined.

The as-sprayed glass coatings are highly defective to be of technical interest: the glass particles, in fact, did not completely flatten on the substrate. A sufficient amount of reinforcing alumina must necessarily be added, at least 40%.

The post-process thermal treatment improves adhesion and cohesion of coating (Fig. 2). It is very important to observe that the coatings obtained with spray-dried alumina possess a microstructure very similar to the ones reinforced with commercial alumina. A too strong process of grit-blasting caused cracks in the substrate.

The SA as-sprayed coatings shows low porosity (6% for SF40), well-flattened splats, no unmelted particles. Also the EA coating, obtained from spray-dried aggregates of very fine platelet-like alumina particles, has a quite compact microstructure, although the porosity is slightly higher than the SA one (10% for EA40). Unfortunately, both coatings have poor adhesion to the stoneware substrate. SF40, SF60, SF80 coatings have similar porosity (6, 7, 7%, respectively), which means that 40% alumina volume fraction is enough to confer good cohesion.

After thermal treatment, the porosity is lightly increased (EF60 passes from 9 to 11%, EF80 from 9 to 15%, SA from 5 to 13%): this is due to the alumina $\gamma \rightarrow \alpha$ phase transformation at high temperature. Since α-Al_2O_3 has a higher density than γ-Al_2O_3, pores and cracks are enlarged. In Figs. 3 and 4 fracture toughness (K_{Ic}) and abrasion rate values (Vn) are reported. Coatings with highest fractions of glass could not be tested, because they were too defective.

Microhardness measurements showed a very high standard deviation: defects, glass splats and alumina splats have completely different resistance to plastic flow, so we can conclude than in this case microhardness is not a useful parameter to evaluate the coatings. Since cracks tend to cross the brittle glass ($K_{Ic} = (0.67 \pm 0.08)$ MPa $m^{1/2}$, cast bulk glass), the smaller the glassy areas, the tougher the coating. 40 vol.% alumina is enough to confer a satisfactory abrasion resistance. The toughness values of EA coating and of spray-dried composite coatings are very similar to the ones manufactured with Sulzer alumina, further indicating the possibility to employ the spray-dried alumina as a less expensive toughening phase.

The wear behaviours are also similar. SF20 and EF20 coatings (too defective for toughness measurements) have much higher Vn values than other composite coatings, indicating that a minimum value of alumina as a reinforcement is necessary to achieve acceptable mechanical properties. In fact, with increasing alumina content, the wear volume decreases non-linearly up to a minimum value for the pure alumina coating, just as fracture toughness. Similar wear volumes were detected for the pure Sulzer alumina and spray-dried alumina samples. Since the thermal treatment improves fracture toughness in the lower alumina content coatings, dry particles abrasion resistance also increases. In the SA, SF80 and EF80 coatings, where the porosity increases in the alumina areas, the abrasion resistance does not increase

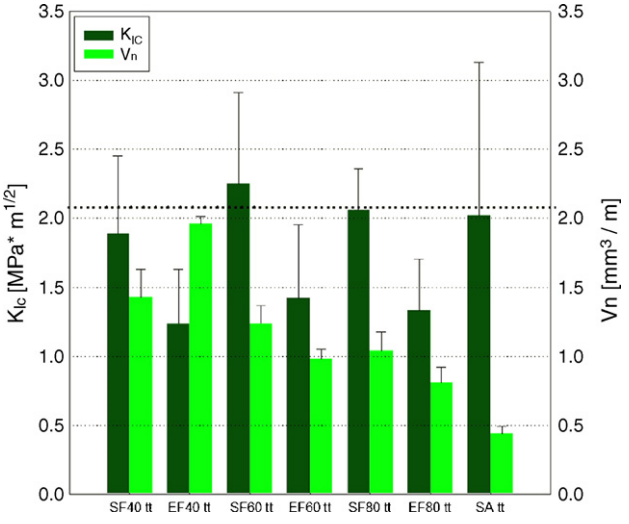

Fig. 4. Mechanical properties of thermally treated coatings. K_{Ic} is fracture toughness, and Vn is the abrasion rate value. Vn = (2.08 ± 0.09) mm^3/m for reference industrial glaze.

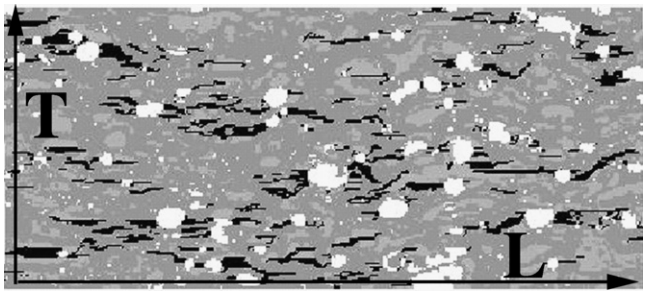

Fig. 5. Simulated cracks from a SEM image by the software OOF of the SF40 tt coating. L = longitudinal axis, and T = transversal axis.

in the same way. The SF80 coating is even weakened by the thermal treatment.

The measured glass mechanical properties[21] have been employed in the numerical modelling. Elastic modulus calculations underline the material anisotropy, with higher elastic modulus in the direction parallel to the substrate (E_T of thermally treated (tt) coatings: SF40 = 158.5 GPa; SF60 = 201.5 GPa; SF80 = 222.2 GPa; E_L of tt coatings: SF40 = 126 GPa; SF60 = 165 GPa; SF80 = 188.2 GPa). Literature studies[22] generally impute the plasma sprayed coatings anisotropy to the low intersplats cohesion (with real intersplat contact area as low as 25% that the nominal one). However, former OOF numerical simulations performed on plasma sprayed coatings have also shown that it is difficult to properly account for the intersplat defects. In this case, the low glass splats roundness (2.4 average elongation, 1.6 average roundness) is another source of anisotropy which the model can certainly reproduce. It is not possible to assess the two contributions to the overall anisotropy; thus, it is uncertain if the numerically predicted anisotropy actually comes from both factors or if the latter one could compensate for the model inability to correctly grasp the intersplat microcracks. Thermal residual stress measurements show that, in all cases, the alumina areas posses an average compressive stress, while glass areas posses an average tensile. The standard deviation is very high on both values, because strong stress intensifications occur near the larger and more irregular pores. Crack propagation modelling studies highlight that cracks start from larger pores and easily propagate through the glass areas, but are stopped by the alumina areas, Fig. 5. This numerical result is completely confirmed by experimental observations on indentation-induced cracks propagation paths. This explains why the fracture toughness should increase if fine glass powders are employed instead of the coarse ones; in fact, smaller glass areas mean less easy propagation paths for cracks. The thermal treatment appears to enhance the ability of alumina to stop crack propagation, because of the increasing of its compressive residual stress: together with the local sintering of glass, this is the reason for the toughness increase after the thermal treatment in many of the coatings.

5. Case study no. 3: high quality plasma sprayed glazes for traditional ceramics

Plasma spraying is a well-known technique for the deposition of ceramic coatings. However, few studies exist concerning plasma spray deposition of glasses, except for biomedical applications.[23] Conventional glazing processes for traditional ceramics have some drawbacks (the same firing temperature and thermal expansion coefficient between glaze and substrate are required) which would be overcome by the employment of plasma spraying. These requirements in standard glazing limit glazes compositions, preventing the employment of systems with high mechanical properties. In plasma spraying, the coating can have higher melting point than the substrate and, being the latter only moderately pre-heated, no major thermal expansion trouble arises. Should a post-process thermal treatment be needed, the treatment temperature would be definitely lower than that of traditional firing processes.

A CZS frit (52% SiO_2, 31% CaO, 16.5% ZrO_2), designed for its ability to form a glass ceramic,[24] and a CAS frit (60% SiO_2, 15% Al_2O_3, 23% CaO) were employed. Frits were wet milled with sintered alumina balls in porcelain jars, simulating a conventional ceramic milling process. The plasma spraying deposition parameters are: 6 mm torch nozzle; 115 mm spray distance; 500 mm/s torch traverse speed; Ar (50 Slpm)/H_2 (14 Slpm) plasma gas mixture; 600 A current and 72 V voltage for a 43.20 kW overall power input; Ar (3 Slpm) as carrier gas. The substrate was cooled with Ar at 7 bar from two nozzles during coating deposition. Thermal treatments were performed on as-sprayed coatings, to sinter the structure and attain the desired crystallization: 15 °C/min heating to 850 °C, 30 min isotherm, 15 °C/min heating to 950 °C, 30 min or 60 min isotherm, cooling inside the furnace (these treatments are hereafter indicated as 9-30 or 9-60, respectively); 15 °C/min heating to 850 °C, 30 min isotherm, 15 °C/min heating to 1050 °C, 15 min or 30 min isotherm, cooling inside the furnace (these treatments are hereafter referred to as 10-30 or 10-15, respectively). For comparative purposes, tests were also performed on porcelainized stoneware and on high-performance industrial glazes, as well as on cast bulk CAS and CZS glass samples. As-sprayed coatings are defective, with ≈10% porosity, but possess good interface with the substrate: in tensile adhesion tests, fracture never occurs at the interface (8 MPa maximum sustained load). CZS 9-30 and 9-60 samples are well-sintered but not crystallized. CZS 10-30 and 10-15 samples are considerably sintered (5% porosity) and largely crystallized with $Ca_2ZrSi_4O_{12}$ micrometric grains in a wollastonite matrix, crystals being smaller and more numerous after the 10-15 treatment. Coating-substrate interface, pores, defects, some limited glass de-mixings and crystallizations occurring during plasma spraying are preferential surface nucleation sites, extending devitrification to the whole coating thickness. The coating interface with the substrate becomes excellent, because the glass infiltrates substrate porosities, and crystals grow from the interface itself. Adhesion is again higher than 8 MPa. CAS 9-30 samples are well-sintered but completely glassy; some pseudowollastonite and anortite appear after the 10-30 treatment, but this crystallization hinders sintering, increasing the overall porosity. Mechanical properties are a consequence of these microstructures. As-sprayed CZS and CAS have lower K_{Ic} (Lankford formula), H_V and E (Table 3) than bulk glass; their abrasion resistance is thus lower than both porcelanized stoneware and industrial glazes due to a very low

Table 3
Mechanical properties for all tested materials

Material	H_V [kg/mm^2] (load in g)	K_{Ic} [MPa m$^{1/2}$]	Wear volume, V_N [mm^3/m]	E [Gpa]
Stoneware	420 ± 46 (25)	1.628 ± 0.475	1.552	72.14
Industrial glaze	415 ± 48 (25)	–	2.080	–
As-sprayed CZS	457 ± 82 (25)	0.371 ± 0.217	3.198	30.62
9-30 CZS	511 ± 78 (25)	1.112 ± 0.141	2.390	–
9-60 CZS	498 ± 44 (25)	0.900 ± 0.165	1.540	–
10-30 CZS	622 ± 99 (50)	2.144 ± 0.446	1.194	109.85
10-15 CZS	594 ± 85 (50)	2.535 ± 0.623	0.720	–
Bulk CZS glass	575 ± 40 (25)	1.584 ± 0.216	–	95.35
Bulk annealed CZS	640 ± 63 (50)	Not measurable	–	–
As-sprayed CAS	401 ± 68 (10)	Not measurable	5.044	–
9-30 CAS	451 ± 63 (25)	1.123 ± 0.146	1.898	–
10-30 CAS	–	–	1.612	–
Bulk CAS glass	515 ± 66 (25)	1.711 ± 0.154	–	83.77

coating cohesion. The main abrasion mechanism is brittle splats detachment. In 9-30 and 9-60 coatings, microhardness and fracture toughness are increased by enhanced cohesion, but not up to bulk glass values. Abrasion resistance increases, approaching the best glazes. Abrasion is mainly due to brittle fracture, with cracks freely propagating in the glass. In 10-30 CAS coating, insufficient crystallization cannot produce significant effects; in 10-30 and 10-15 CZS coatings the large crystallization increases H_V (approaching annealed bulk CZS surface), E and K_{Ic} (higher than bulk CZS glass and porcelanized stoneware). Thus, the potential benefits offered by crystallization are fully exploited. Higher K_{Ic} explains the better abrasion resistance than porcelanized stoneware: frequent deflections due to several small crystals obstacle crack propagation. 10-15 CZS coating, characterized by more numerous and smaller grains, is slightly less hard but tougher, which explains its higher abrasion resistance.

After the acid resistance test, no substantial change is optically visible on coatings and stoneware surfaces. With methylene blue treatment, minimum effects appear on porcelanized stoneware; a marked colour difference is perceivable in as-sprayed coatings (open porosity enhances chemical reactivity of the glass); on industrial glazes and 10-30 CZS coatings, a slight colour difference still exists. In crystallized CZS, wollastonite is selectively dissolved due to its intrinsically poor chemical resistance: this is an unavoidable limit of the CZS system.

6. Conclusions

Plasma spraying and the other techniques belonging to the thermal spraying group are usually applied to coat metallic substrates, but they could be very useful to improve the properties of the surface of ceramic materials. To support this statement, three case studies concerning plasma sprayed coatings on traditional ceramic substrates have been presented. The first case concerned the improvement of the corrosion resistance to molten glass of porous low cost refractories: preliminary results are very promising, even though further work must be done to increase thermal shock resistance and longer tests in contact with molten glass at high temperature should be carried out. In the other two examples, porcelainized stoneware tiles have been coated with an alumina-glass composite thick layer and with high quality industrial frits. In the former case, a considerable amount of waste glass has been used (up to 60%), that is to say "recycled", together with a low cost alumina as reinforcement, to produce coatings with properties similar to commercial traditional glazes. In the latter case, exploiting the pre-sintering status which plasma spraying has provided to the glass frits as-sprayed coatings, high quality glass and glass ceramic coatings have been manufactured by means of relatively low temperatures post deposition thermal treatments (950 and 1050 °C). The researches shown in this paper are still at the laboratory scale and many industrial tests should be performed in order to assess the applicability of thermal spraying techniques to the production processes. Nevertheless, the great versatility of these coating methods as far as the coating materials and equipments are concerned are very promising for many traditional ceramic applications.

Acknowledgements

The authors are grateful to Ing. F. Casadei, E. Severini and V. Ferretti for the spraying runs in Centro Sviluppo Materiali, Roma. The authors wish to thank Chiara Venturelli (Expert System Solutions, Modena) for the precious CTE measurements. Many thanks to the colleagues of Dipartimento di Ingegneria dei Materiali e dell'Ambiente (Università di Modena e Reggio Emilia): Ing. Giovanni Bolelli for the experimental work, Prof. L. Barbieri, Dr. I. Lancellotti and Dr. F. Andreola for their consultancy in materials recycling, Prof. V. Cannillo for FEM calculations and Prof. C. Siligardi for her advices in glass coating analysis. Partially supported by PRRIITT (Regione Emilia Romagna), Net-Lab "Surface & Coatings for Advanced Mechanics and Nanomechanics" (SUP&RMAN).

References

1. Herman, H., Sampath, S. and McCune, R., Thermal spray: current status and future trends. In *Thermal Spray Processing of Materials*, ed. S. Sampath and P. McCune. MRS Bull., 2000, pp. 17–25.
2. Vardelle, A., Fauchais, P., Dussoubs, B. and Themelis, N. J., Heat Generation and Particle Injection in a Thermal Plasma Torch. *Plasma Chem. Plasma Process.*, 1998, **18**, 551–572.

3. Matejicek, J., Sampath, S., Gilmore, D. and Neiser, R., In situ measurement of residual stresses and elastic moduli in thermal sprayed coatings. Part 2. Processing effects on properties of Mo coatings. *Acta Mater.*, 2003, **51**, 873–885.
4. Ctibor, P., Roussel, O. and Tricoire, A., Unmelted particles in plasma sprayed coatings. *J. Eur. Ceram. Soc.*, 2003, **23**, 2993–2999.
5. Heimann, R. B., Applications of plasma-sprayed ceramic coatings. *Key Eng. Mater.*, 1996, **122–124**, 399–442.
6. Bolelli, G., Cannillo, V., Lusvarghi, L., Manfredini, T., Siligardi, C., Bartuli, C., Loreto, A. and Valente, T., Plasma-sprayed glass-ceramic coatings on ceramic tiles: microstructure, chemical resistance and mechanical properties. *J. Eur. Ceram. Soc.*, 2005, **25**, 1835–1853.
7. Ponton, C. B. and Rawlings, R. D., Vickers indentation fracture toughness test. Part 1. Review of literature and formulation of standardised indentation toughness equations. *Mater. Sci. Technol.*, 1989, **5**, 865–872.
8. Ponton, C. B. and Rawlings, R. D., Vickers indentation fracture toughness test. Part 2. Application and critical evaluation of standardised indentation toughness equations. *Mater. Sci. Technol.*, 1989, **5**, 961–976.
9. Jorge Lino, F., Duarte, T. P. and Maia, R., Development of coated ceramic components for the aluminium industry. *J. Thermal Spray Technol.*, 2003, **12**, 250–257.
10. Li, J. F., Li, L. and Stott, F. H., Multi-layered surface coatings of refractory ceramics prepared by combined laser and flame spraying. *Surf. Coat. Technol.*, 2004, **180–181**, 500–505.
11. Ono, T., *Refractories Handbook*. The Technical Association of Refractories, Japan, Tokyo, 1998, pp. 446–455.
12. Gibson, R. F., *Principles of Composite Material Mechanics*. Singapore, McGraw-Hill, 1994.
13. Rohan, P., Neufuss, K., Matejicek, J., Dubsky, J., Prchlik, L. and Holzgartner, C., Thermal and mechanical properties of cordierite, mullite and steatite produced by plasma spraying. *Ceram. Inter.*, 2004, **30**, 597–603.
14. Widjaja, S., Limarga, A. M. and Yip, T. H., Modeling of residual stresses in a plasma-sprayed zirconia/alumina functionally-graded thermal barrier coating. *Thin Solid Films*, 2003, **434**, 216–227.
15. Hreglich, S., Falcone, R. and Vallotto, M., In *The Recycling of End of Life Panel Glass from tv Sets in Glass Fibres and Ceramic Productions – Recycling and Reuse of Glass Cullet*, ed. Telford, 2001, pp. 123–134.
16. Doring, E., "To get new picture tubes from old ones", pp. 1–34, http://www.uiah.fi/klo/research/kimokela/To_get_new_picture_tubes_presentation.ppt.
17. Langer, S. A., Fuller, E. R. and Carter, W. C., OOF: an image-based finite element analysis of material microstructures. *Comput. Sci. Eng.*, 2001, **3**, 15–23.
18. Zimmermann, A., Fuller Jr., E. R. and Rödel, J., Residual stress distributions in ceramics. *J. Am. Ceram. Soc.*, 1999, **82**(11), 3155–3160.
19. Zimmermann, A., Carter, W. C. and Fuller Jr., E. R., Damage evolution during microcracking of brittle solids. *Acta Mater.*, 2001, **49**(1), 127–137.
20. Wang, Z., Kulkarni, A., Deshpande, S., Nakamura, T. and Herman, H., Effects of pores and interfaces on effective properties of plasma sprayed zirconia coatings. *Acta Mater.*, 2003, **51**(18), 5319–5334.
21. Barbieri, L., Bolelli, G., Cannillo, V., Lusvarghi, L., Riccò, S. Computational simulation and experimental characterization of the mechanical and fracture behaviour of alumina-glass plasma sprayed coatings. In *International Thermal Spray Conference & Exposition*, ed. E. Lugscheider. Dusseldorf, 2005, pp. 357–362.
22. Damani, R. J. and Wanner, A., Microstructure and elastic properties of plasma-sprayed alumina. *J. Mater. Sci.*, 2000, **35**, 4307–4318.
23. Schrooten, J. and Helsen, J. A., Adhesion of bioactive glass coating to Ti6Al4V oral implant. *Biomaterials*, 2000, **21**, 1461–1469.
24. Siligardi, C., D'Arrigo, M. C. and Leonelli, C., Densification of glass powders belonging to the CaO-ZrO_2-SiO_2 system by microwave heating. *J. Eur. Ceram. Soc.*, 2000, **20**(2), 177–183.